JOURNAL OF SPACECRAFT AND ROCKETS
Vol. 33, No. 4, July–August 1996

Heat Transfer in Two-Phase Solid-Rocket Plumes

H. F. Nelson* and John C. Fields†
University of Missouri–Rolla, Rolla, Missouri 654019-0050

Results of a direct simulation Monte Carlo (DSMC) and free molecule (FM) analysis of convective heat transfer to Al_2O_3 particles in solid-rocket plume environments are presented. The particle diameters are assumed to be 4μm, and the plume gases are CO_2, H_2O, CO, and N_2. The plume gas temperature is 2000 K. Particle temperatures of 1500, 2000, and 2500 K are investigated for Knudsen numbers from $\frac{1}{2}$ to 1000 (from slip flow to FM flow). The Nusselt number is presented in terms of Knudsen number and Reynolds number (or relative velocity). Both the Kavanau and the Kashmarov and Svirshevskii correlations generally agree with the DSMC and FM predictions of the particle Nusselt numbers. Vibrational excitation of the gas molecules is an important effect in the prediction of the particle adiabatic wall temperature. To the authors' knowledge, this paper presents the first correlations of Nusselt number and adiabatic wall temperature for high-temperature plume gases.

Nomenclature

A = particle surface area, πD^2
a = speed of sound, m/s
C_p, C_v = gas specific heat at constant pressure, volume, J/(kg·K)
D = particle diameter, μm
f_{Nu} = normalized Nu; see Eq. (14)
h = convective heat transfer coefficient, W/(m²·K)
j_r = rotation energy, RT units
j_v = gas vibration energy, RT units
Kn = Knudsen number $= \lambda/D$
k = gas thermal conductivity, W/(m·K)
k_B = Boltzmann's constant, 1.3807×10^{-23} J·s
M = relative Mach number, U/a
N = number density, cm^{-3}
Nu = Nusselt number, hD/k
Nu_{fm} = free-molecule-flow Nu; see Eq. (8)
n = number of collisions in a cell
Pr = Prandtl number, $C_p\mu/k$
$\dot{Q}$ = convective heat transfer rate, W
$\dot{q}$ = convective heat flux, W/m²
R = specific gas constant
Re = Reynolds number, $\rho U D/\mu$
S = speed ratio, $\sqrt{(\gamma/2)}M$
T = temperature, K
T_0 = total temperature, K
U = relative velocity, $U_g - U_p$, m/s
Z = parameter; see Eq. (9)
z = distance along plume centerline, m
α = accommodation coeffficient = 1
β_c = continuum-flow Nu; see Eq. (10)
β_{fm} = free-molecule-flow Nu; see Eqs. (11) and (13)
γ = ratio of specific heats, C_p/C_v
$\theta_{v,i}$ = energy of ith vibration mode, K
λ = gas mean free path, μm
μ = gas dynamic viscosity, N·s/m²
ρ = gas density, kg/m³

Subscripts

ad = adiabatic wall value
g = gas
p = particle

Presented as Paper 95-2131 at the AIAA 29th Thermophysics Conference, San Diego, CA, June 19–22, 1995; received Aug. 4, 1995; revision received Oct. 25, 1995; accepted for publication Nov. 1, 1995.

*Professor of Aerospace Engineering, Thermal Radiative Transfer Group, Department of Mechanical and Aerospace Engineering and Engineering Mechanics. Associate Fellow AIAA.
†Graduate Student, Department of Mechanical and Aerospace Engineering and Engineering Mechanics.

Introduction

EXHAUST plumes of aluminum-fueled solid rocket motors contain a large number of liquid and solid aluminum oxide particles. Prediction of solid-rocket plume flowfields and radiative emission depends on accurate modeling of heat transfer between particulates and plume gases. Radiation emitted by the plume is dominated by continuum emission from Al_2O_3 particles, and its magnitude is very sensitive to particle temperature. The particle temperature is, in turn, a strong function of heat transfer between the particles and the plume gases. The rate at which particles exchange heat by convection and radiation with the plume gases determines their temperature. In this paper the radiative heat transfer is neglected, and the convective heat transfer to the particle is

$$\dot{Q} = hA(T_{\text{ad}} - T_p) \tag{1}$$

The heat transfer goes to zero when $T_p = T_{\text{ad}}$. The particle transfers heat to the gas when T_p is larger than T_{ad}. The heat transfer coefficient h is given in terms of the Nusselt number.

Moylan and Sulyma[1] studied the accuracy of current Nu prediction models for convective heat transfer in Al_2O_3 particulate solid-rocket plumes. They pointed out that current plume flowfield prediction codes use $T_g - T_p$, instead of $T_{\text{ad}} - T_p$, for convective heat transfer calculations. Use of $T_g - T_p$ is correct if the relative velocity between the gas and the particles is zero. However, there is an appreciable relative velocity between the gas and the particles in plumes, so the driving temperature difference should be the difference between the adiabatic wall temperature (recovery temperature) and the particle temperature, so that $\dot{Q}$ goes to zero when $T_p = T_{\text{ad}}$. They also showed that the Kavanau (Kav) correlation, which extends a continuum-flow relation to slip flow, provides an adequate Nu prediction for plume flows. However, they used 300 K air as the plume gas in their analysis.

The objective of the present research is to numerically predict Nu for plume gases (CO_2, H_2O, CO, and N_2) at realistic plume temperatures and pressures.

Kavanau Correlation

Kavanau[2] conducted experiments to determine Nu for spheres in subsonic, rarefied airflow at low temperatures (300 K). He correlated Nu for rarefied flow by applying a correction to Nu for continuum flow at the same Reynolds number. His method is currently employed in many computational codes. The Kav correlation is

$$Nu = \frac{Nu_c}{1 + 3.42(M/Re\,Pr)Nu_c} \tag{2}$$

where Nu_c is the Nusselt number for continuum flow over a sphere.[3] It is defined as

$$Nu_c = 2 + 0.459\, Re^{0.55}\, Pr^{0.33} \tag{3}$$

Free-Molecule Flow

Sauer[4] and Oppenheim[5] published free-molecule (FM)-flow predictions of convective heat transfer and recovery factors for flow over several simple shapes, including spheres. Their analysis applies to low-temperature situations, where γ is constant. In other words, they did not consider vibrational excitation of the gas molecules. This work is extended in the current research to include vibrational excitation, because the plume gas temperatures of interest are of the order of 2000 K. Following the work of Oppenheim, the nondimensional convective flux becomes

$$\frac{\dot{q}}{\alpha N_g k_B T_g U} = -\left[(2 + j_r + j_{v,p})(\bar{G} + \bar{F})\frac{T_p}{T_g} - \left(S^2 + \frac{5}{2} + j_r + j_{v,g}\right)(\bar{G} + \bar{F}) + \frac{1}{2}\bar{G}\right] \tag{4}$$

The net heat transfer rate over the entire particle is $\dot{Q} = \int_A \dot{q}\, dA$. The parameter j_r is 1 for CO, N_2 and CO_2, and 1.5 for H_2O. The value of j_v is different for incident and reflected molecules. For the harmonic oscillator model, it is

$$j_v = \sum_{i=1}^{I} \frac{\theta_{v,i}/T}{\exp(\theta_{v,i}/T) - 1} \tag{5}$$

so that the vibration energy per molecule is $e_v = j_v k_B T$, where T is T_g for incident or T_p for reflected molecules, because the molecules are fully accommodated at the particle surface. $I = 1$ for N_2 and CO, because these molecules have only one vibrational state. We have $\theta_{v,i} = 3390$ and 3070 K for N_2 and CO, respectively. H_2O has three vibrational modes ($I = 3$) with $\theta_v = 2294$, 5262, and 5404 K, and CO_2 has four vibrational modes ($I = 4$) with $\theta_v = 1932$, two at 960, and 3380 K. Note that the numbers of degrees of freedom in rotation and vibration are $2j_r$ and $2j_v$, respectively.

For spherical particle, the functions $\bar{G}$ and $\bar{F}$ are

$$\bar{G} = \frac{\text{erf}(S)}{4S^2} \tag{6}$$

and

$$\bar{F} = \frac{1}{4}\left[\frac{\exp(-S^2)}{\sqrt{\pi}S} + \frac{2S^2 - 1}{2S^2}\,\text{erf}(S)\right] \tag{7}$$

T_{ad} is obtained by setting $\dot{q} = 0$ in Eq. (4) and solving for T_p such that $T_p = T_{ad}$. In FM flow with vibrational excitation, both $\dot{Q}$ and T_{ad} become functions of j_v; thus, an iterative solution is required. For FM flow with no vibrational excitation, T_{ad} is determined by setting $j_v = 0$. The resulting FM Nusselt number becomes

$$Nu_{fm} = \alpha\frac{\gamma - 1}{\gamma}\, Pr\, Re\, \frac{\bar{G} + \bar{F}}{T_{ad} - T_p} \times [(2 + j_r + j_{v,ad})T_{ad} - (2 + j_r + j_{v,p})T_p] \tag{8}$$

In Eqs. (2) and (8), the parameters γ, Pr, M, and Re are evaluated at T_g. If the flow were continuum, these parameters would be evaluated at the reference temperature.[6]

Koshmarov–Svirshevskii Correlation

Koshmarov and Svirshevskii[7] conducted experiments and correlated other experimental data to develop an empirical correlation equation for convective heat transfer for spheres at subsonic, transonic, and supersonic Mach numbers in slip and rarefied flows. Their experiments and correlations dealt only with air at temperatures of approximately 300 K. They developed a Nu correlation, which is more complicated than that of Kavanau,[2] as well as a T_{ad} correlation.

Koshmarov and Svirshevskii[7] developed their correlation in terms of a dimensionless parameter

$$Z = \frac{8\beta_c}{\beta_{fm} + 4\beta_c} \tag{9}$$

where the continuum Nu is

$$\beta_c = 2 + 0.03 Pr_0^{0.33} Re_0^{0.54} + 0.35 Pr_0^{0.356} Re_0^{0.58} \tag{10}$$

where Re_0 and Pr_0 are the Reynolds and Prandtl numbers with μ and k evaluated at T_0 ($= T_g[1 + (\gamma - 1)S^2/\gamma]$) instead of T_g and β_{fm}, the FM Nu, follows from Eq. (8) for a diatomic gas ($j_r = 1$) and no vibrational excitation ($j_{v,ad} = j_{v,g} = 0$):

$$\beta_{fm} = \alpha(\gamma - 1/\gamma)\tfrac{3}{4}(Pr\, Re/S^2)\phi(S) \tag{11}$$

The function $\phi(S) = 4S^2(\bar{G} + \bar{F})$, or

$$\phi(S) = \left(\frac{1}{2} + S^2\right)\text{erf}(S) + \frac{S\exp(-S^2)}{\sqrt{\pi}} \tag{12}$$

In Ref. 7 and its original Russian version, β_{fm} is written slightly differently from the FM result in Eq. (11). It is written as

$$\beta_{fm} = \alpha(\gamma + 1)\frac{Pr_0 Re_0}{2S^2}\phi(S) \tag{13}$$

In the current work, Eq. (13) with γ evaluated at T_g is used for β_{fm} in the Koshmarov–Svirshevskii (K–S) correlation.

The normalized Nu is defined in terms of Z as

$$f_{Nu} = \frac{Z}{1 + (Z/2)^{1.5}} \tag{14}$$

Thus f_{Nu} ranges from approximately 0 for continuum flow to about 2 for FM flow. Nu predicted by the K–S correlation is

$$Nu = f_{Nu}(Nu_{fm} + \beta_c) - \beta_c \tag{15}$$

It can be shown by using Eq. (8) in Eq. (15) that Nu goes to 0 as β_{fm} goes to 0, and that Nu goes to 14 as β_c goes to 2 and β_{fm} goes to infinity. In addition the K–S method predicts T_{ad} as

$$T_{ad} = \sqrt{Pr_0}(T_0 - T_g) + T_g \tag{16}$$

for laminar flow.

Plume Properties

Typical ranges for plume parameters are determined from plume flowfield solutions obtained from Hiers[8] for the Orbus I solid rocket motor at maximum thrust of 27,000 N at an altitude of 67 km and a velocity of 513 m/s, or Mach 1.6. Centerline gas properties at the nozzle exit were $U_g = 2416$ m/s, $T_g = 2110$ K, $P_g = 0.1538$ atm, gas number density $= 5.349 \times 10^{17}$ cm^{-3}, and gas Mach number = 2.20. The gas mole fractions were CO = 0.2470, CO_2 = 0.0158, Cl = 0.0103, H = 0.0376, H_2 = 0.3256, H_2O = 0.1142, HCl = 0.1220, OH = 0.0015, and N_2 = 0.1257. Other gases (Cl_2, O, and O_2) were present, but in much smaller mole fractions. Particles at the nozzle exit were divided into three size groups, based on particle diameter, with the following properties: $D = 2.53\,\mu$m ($T = 2463$ K, $U_p = 2256$ m/s, $N_p = 237,500$ cm^{-3}); $D = 4.71\,\mu$m ($T = 2638$ K, $U_p = 2094$ m/s, $N_p = 72,770$ cm^{-3}); $D = 8.76\,\mu$m ($T = 2857$ K, $U_p = 1819$ m/s, $N_p = 31,340$ cm^{-3}). The Orbus I motor has an exit diameter of 37.7 cm and a throat diameter of 5.5 cm, which corresponds to a nozzle expansion ratio of 46.3.

Figure 1 shows T_g and T_p as a function of z. We see that T_g drops rapidly after the gas exits the nozzle, because of the rapid expansion. T_g increases to about 3000 K as the gas passes through the Mach disk at about 50 m downstream of the nozzle exit. Beyond the Mach disk, T_g generally decreases on account of plume expansion, although some oscillations occur due to reflected shocks from the plume boundaries. In the expansion at the nozzle exit, the plume gases quickly drop to temperatures below 300 K, yet they may remain

vibrationally excited because the collisional deexcitation processes become frozen. Thus, the vibrational states and the translational–rotational states tend to be in thermal nonequilibrium. These effects are not considered. Only equilibrium population of the vibrational states is considered in this paper.

Particles leave the nozzle in the liquid state, and T_p quickly drops to near the solidification temperature of 2317 K. T_p remains constant during the solidification process. Once solidification is complete, T_p begins to decrease again. Note that the smaller particles solidify much faster than the larger ones.

Figure 2 shows normalized gas and particle number densities on the plume centerline as a function of z. We see that N_g decreases between the nozzle exit and the Mach disk on account of plume expansion, then increases behind the Mach disk and becomes relatively constant in the far plume. Centerline N_p values decrease with increasing distance from the nozzle in the near plume. In the far plume, N_p becomes constant because the particle diffusion rates reach equilibrium.

Figure 3 shows U on the plume centerline as a function of z. We see that U_g is greater than U_p between the nozzle exit and the Mach disk. At the Mach disk, U_g is greatly reduced, while U_p is unchanged because the particles are not affected by the shock wave. Also, Fig. 1 shows that T_p is not changed as the particles pass through the Mach disk. The particle velocity is as much as 2000 m/s faster than the gas velocity just behind the Mach disk. Behind the Mach disk, U gradually goes to a value of about −500 m/s. The particle size affects U, with the smaller particles generally following U_g more closely than the larger ones.

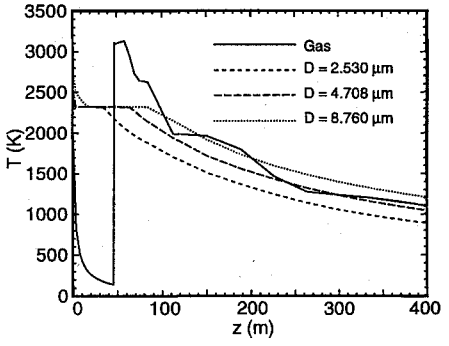

Fig. 1 Centerline T_g and T_p vs z.

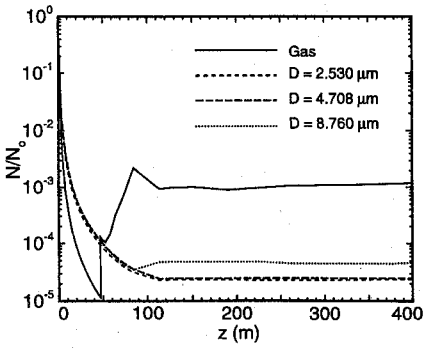

Fig. 2 Centerline normalized number density of gas and particles vs z, where $N_0 = 5.349 \times 10^{17}$ cm^{-3} for gas, and N_0 = 237,500, 72,770, and 31,340 cm^{-3} for D = 2.530-, 4.708-, and 8.760-μm particles, respectively.

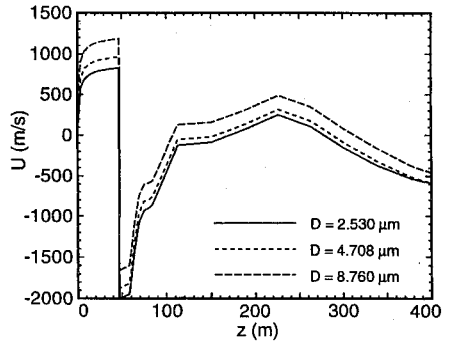

Fig. 3 Centerline relative velocity ($U_g - U_p$) vs z.

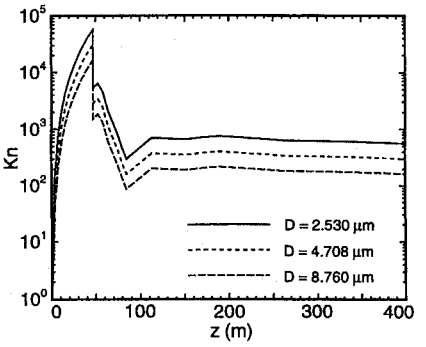

Fig. 4 Centerline *Kn* vs z.

Figure 4 shows the centerline Knudsen number as a function of z. A representative gas molecule diameter of $d = 5.0 \times 10^{-10}$ m was used to calculate λ $\{=1/[\sqrt{(2\pi)}d^2N_g]\}$ for the Kn data. Kn varies from 0.10 at the nozzle exit to 80,000 at the Mach disk. It stays relatively constant between 100 and 800, depending on the particle size behind the Mach disk. Clearly, the plume particles are in the slip and rarefied flow regimes.

Direct Simulation Monte Carlo Method

In the direct simulation Monte Carlo (DSMC) method, intermolecular collisions are considered on a probabilistic basis. Billions of gas molecules are represented computationally by hundreds of simulated molecules. All calculations are unsteady and are started from an initial state of uniform equilibrium flow. A computational cell network is required in physical space and is used to facilitate the choice of potential collision pairs and the sampling of the macroscopic flow properties.

Velocity components, internal energy values, and position coordinates of the molecules are stored and modified with time as the molecules undergo collisions and boundary interactions in simulated physical space. Time in the simulation may be identified with physical time in the real flow. The computational time is directly proportional to the number of simulated molecules. The variable hard sphere (VHS) molecular model was used to model the molecules. More information about DSMC and VHS is given in Refs. 9 and 10.

The flowfield is modeled as a two-dimensional axisymmetric flow over a spherical Al_2O_3 particle with $D = 4\,\mu$m. The DSMC grid extended 10 particle radii out from the center of the particle. There were 20 cells in both the radial and angular directions, for a total of 400 cells in the flowfield. Weighting factors, a program option, were used in the calculations to ensure that the cells near the particle contained an adequate number of molecules. Ideally, one would like 5–20 molecules in every cell. For the 400-cell grid all of the cells contained at least 4 molecules.

DSMC adds the number of surface collisions as they occur. The code was run until the molecules in every cell at the particle surface had undergone 6000 or more collisions with the surface. All molecules were fully accommodated at the surface. During this time the molecules in the outer cells had undergone millions of collisions. The statistical error decreases as $1/\sqrt{n}$. Thus, for $n = 6000$ or more, the error was of the order of 1.5% or less. (For most cases n was greater than 10,000.)

In the DSMC calculations, the gas vibrational modes were modeled as additional degrees of freedom in rotation. For equilibrium vibrational population at 2000 K, the numbers used for the sum of j_r and j_v were 2.83, 7.10, 4.86, and 2.76 for CO, CO_2, H_2O, and N_2, respectively. The average number of collisions to relax the vibration–rotation modes was assumed to be 5. In addition, the viscosity data necessary for the VHS molecular model were fitted using a reference temperature of 1500 K. The best fit yielded values of the viscosity index (nondimensional) and reference viscosity (N·s/m^2)

of 0.63 and 5.16×10^{-5}, 0.73 and 5.20×10^{-5}, 1.10 and 5.76×10^{-5}, and 0.62 and 5.12×10^{-5} for CO, CO_2, H_2O, and N_2, respectively.

DSMC is normally applied to situations in which the molecule kinetic and thermal energies are of the same order. In the current application this was not true. The sensible enthalpy of each of the gases at 2000 K is roughly CO_2 2100, CO 2000, N_2 2000, and H_2O 4000 kJ/kg. The kinetic energy is 5, 125, and 500 kJ/kg for velocities of 100, 500, and 1000 m/s, respectively. Thus, the ratio of kinetic to thermal energy is 0.0024, 0.0025, 0.0025, and 0.00125 for CO_2, CO, N_2, and H_2O, respectively, at 100 m/s. The ratio will be a factor of 100 greater for velocities of 1000 m/s. The small ratio of kinetic to thermal energy seemed to increase the statistical variation of the DSMC solutions, and increased the computer run time to obtain solutions. Convergence of H_2O solutions at 100 m/s was particularly difficult to obtain. The computer time to obtain solutions varied greatly with the type of computer used. For a personal computer with a 486 processor, solutions required about 175 h of CPU time. A Sun workstation was roughly three times as fast, requiring about 60 h of CPU time.

Methodology

DSMC calculations were done for representative plume conditions based on data shown in Figs. 1–4.[11] The particle diameter was fixed at 4 μm, and the gas temperature was fixed at 2000 K. Flow velocities of 100, 500, and 1000 m/s were used, and T_p values of 1500, 2000, and 2500 K were considered. N_g was determined so that Kn was either $\frac{1}{2}$, 1.0, or 2.0. Thus, the DSMC calculations were in the slip flow regime. FM calculations were done for Kn from $\frac{1}{2}$ to 1000. DSMC and FM results were compared at $Kn = \frac{1}{2}$, 1, and 2. The gases considered were CO_2, CO, H_2O, and N_2. These gases generally have the highest mole fraction in the plume. Most of the previous Nu calculations were done for air at around 300 K, so this work extends the state of the art to include high-temperature gases and gases other than air.

Results and Discussion

T_{ad} must be known prior to determining Nu [see Eq. (1) and the definition of Nu]. For DSMC this was done by a trial-and-error method consisting in running several cases for different values of T_p and obtaining the value of $\dot{Q}$. Plots of $\dot{Q}$ vs T_p were used to determine T_{ad}, which is the value of T_p at which $\dot{Q} = 0$. This method became inaccurate when T_{ad} was close to T_p, say within 10 K, because an error of 1 K out of 2000 K produced an error of 10% in $\dot{Q}$. If T_{ad} was less than T_0, then T_{ad} was assumed equal to T_0. The details are given in Ref. 11. For the FM cases, T_{ad} could be determined from Eq. (4) with $\dot{q} = 0$.

Tables 1–4 present Nu data for CO_2, CO, N_2, and H_2O, respectively. Each table shows Nu data for $U = 100$, 500, and 1000 m/s as a function of Kn for $T_g = 2000$ K. T_p was varied between 1500 and 2500 K for each Kn value for the DSMC calculations. $T_p = 2000$ K for the free molecule (FM) calculations. The first three columns contain Kn, Re, and T_{ad}. The next five columns contain Nu for DSMC the FM theory, the FM theory with no vibrational excitation (FM*), the Kav correlation, and the K–S correlation. DSMC calculations of Nu were done at $Kn = \frac{1}{2}$, 1, and 2 as listed in the tables. Values of Nu at larger Kn are from FM theory. DSMC results were averaged over a set of results at each Kn and U. Each set contained Nu results at T_p between 1500 and 2500 K. The DSMC value listed in the tables represents an average over 1 to 6 cases at each Kn and U. The largest standard deviation in Nu (as a percentage of average Nu) was 14.1% for H_2O at $Kn = 2$ and $U = 500$ m/s; 11.6% for CO_2 at $Kn = \frac{1}{2}$ and $U = 500$ m/s; 6.6% for CO at $Kn = \frac{1}{2}$ and $U = 500$ m/s; and 10.6% for N_2 at $Kn = 2$ and $U = 500$ m/s. T_{ad} is a function of Kn for the DSMC calculations, so the DSMC value of T_{ad} is given where available. In FM flow T_{ad} is independent of Kn. Note that the Kav and the K–S correlations yield similar Nu values for each gas.

Comparisons of DSMC and the K–S correlation were developed using the parameters Z and f_{Nu} from Eqs. (9) and (14) for the DSMC-case conditions. Values for Nu and T_{ad} for the K–S correlation were calculated using Eqs. (15) and (16).[11]

Table 1 Nusselt numbers for CO_2

			Nu				
Kn	Re	T_{ad}	DSMC	FM	FM*[a]	Kav	K–S
			$U = 100$ m/s				
0.5	0.4796	2004	0.5810	0.7553	0.3391	0.5013	0.4303
1.0	0.2398	2005	——	0.3776	0.1696	0.2804	0.2378
2.0	0.1199	2005	——	0.1888	0.0848	0.1495	0.1256
5.0	0.0480	2005	——	0.0755	0.0339	0.0624	0.0520
10	0.0240	2005	——	0.0378	0.0170	0.0317	0.0263
20	0.0120	2005	——	0.0189	0.0085	0.0160	0.0132
50	0.0048	2005	——	0.0076	0.0034	0.0064	0.0053
100	0.0024	2005	——	0.0038	0.0017	0.0032	0.0027
1000	0.0002	2005	——	0.0004	0.0002	0.0003	0.0003
			$U = 500$ m/s				
0.5	2.3979	2115	0.4962	0.8309	0.3722	0.5179	0.4895
1.0	1.1989	2132	0.3016	0.4155	0.1861	0.2843	0.2672
2.0	0.5995	2138	0.1581	0.2077	0.0931	0.1503	0.1405
5.0	0.2398	2127	——	0.0831	0.0372	0.0625	0.0581
10	0.1199	2127	——	0.0415	0.0186	0.0317	0.0294
20	0.0599	2127	——	0.0208	0.0093	0.0160	0.0148
50	0.0240	2127	——	0.0083	0.0037	0.0064	0.0059
100	0.0120	2127	——	0.0042	0.0019	0.0032	0.0030
1000	0.0012	2127	——	0.0004	0.0002	0.0003	0.0003
			$U = 1000$ m/s				
0.5	4.7958	2509	06303	1.0511	0.4681	0.5285	0.6410
1.0	2.3979	2468	——	0.5255	0.2341	0.2869	0.3491
2.0	1.1989	2468	——	0.2628	0.1170	0.1509	0.1835
5.0	0.4796	2468	——	0.1051	0.0468	0.0626	0.0759
10	0.2398	2468	——	0.0526	0.0234	0.0317	0.0384
20	0.1199	2468	——	0.0263	0.0117	0.0160	0.0193
50	0.0480	2468	——	0.0105	0.0047	0.0064	0.0078
100	0.0240	2468	——	0.0053	0.0023	0.0032	0.0039
1000	0.0024	2468	——	0.0005	0.0002	0.0003	0.0004

[a]No vibrational excitation.

Table 2 Nusselt numbers for CO

			Nu				
Kn	Re	T_{ad}	DSMC	FM	FM*[a]	Kav	K–S
			$U = 100$ m/s				
0.5	0.3826	2004	0.6804	0.7289	0.5716	0.5279	0.3812
1.0	0.1913	2006	——	0.3644	0.2858	0.2978	0.2143
2.0	0.0956	2006	——	0.1822	0.1429	0.1596	0.1143
5.0	0.0383	2006	——	0.0729	0.0572	0.0668	0.0476
10	0.0191	2006	——	0.0364	0.0286	0.0340	0.0241
20	0.0096	2006	——	0.0182	0.0143	0.0171	0.0122
50	0.0038	2006	——	0.0073	0.0057	0.0069	0.0049
100	0.0019	2006	——	0.0036	0.0029	0.0034	0.0024
1000	0.0002	2006	——	0.0004	0.0003	0.0003	0.0002
			$U = 500$ m/s				
0.5	1.9128	2097	0.5962	0.7769	0.6077	0.5449	0.4250
1.0	0.9564	2122	0.3288	0.3885	0.3039	0.3018	0.2351
2.0	0.4782	2139	0.1619	0.1942	0.1519	0.1605	0.1245
5.0	0.1913	2143	——	0.0777	0.0608	0.0669	0.0517
10	0.0956	2143	——	0.0388	0.0304	0.0340	0.0262
20	0.0478	2143	——	0.0194	0.0152	0.0171	0.0132
50	0.0191	2143	——	0.0078	0.0061	0.0069	0.0053
100	0.0096	2143	——	0.0039	0.0030	0.0034	0.0027
1000	0.0010	2143	——	0.0004	0.0003	0.0003	0.0003
			$U = 1000$ m/s				
0.5	3.8257	2505	0.5711	0.9212	0.7162	0.5561	0.5353
1.0	1.9128	2535	——	0.4606	0.3581	0.3046	0.2933
2.0	0.9564	2535	——	0.2303	0.1791	0.1611	0.1546
5.0	0.3826	2535	——	0.0921	0.0716	0.0670	0.0641
10	0.1913	2535	——	0.0461	0.0358	0.0340	0.0325
20	0.0956	2535	——	0.0230	0.0179	0.0171	0.0163
50	0.0383	2535	——	0.0092	0.0072	0.0069	0.0066
100	0.0191	2535	——	0.0046	0.0036	0.0034	0.0033
1000	0.0019	2535	——	0.0005	0.0004	0.0003	0.0003

[a]No vibrational excitation.

Table 3 Nusselt numbers for N_2

			Nu				
Kn	*Re*	T_{ad}	DSMC	FM	FM*[a]	Kav	K–S
			$U = 100$ m/s				
0.5	0.3826	2004	0.6679	0.7019	0.5553	0.5135	0.3695
1.0	0.1913	2006	——	0.3510	0.2777	0.2887	0.2070
2.0	0.0956	2006	——	0.1755	0.1388	0.1544	0.1102
5.0	0.0383	2006	——	0.0702	0.0555	0.0646	0.0458
10	0.0191	2006	——	0.0351	0.0278	0.0328	0.0232
20	0.0096	2006	——	0.0175	0.0139	0.0165	0.0117
50	0.0038	2006	——	0.0070	0.0056	0.0066	0.0047
100	0.0019	2006	——	0.0035	0.0028	0.0033	0.0024
1000	0.0002	2006	——	0.0004	0.0003	0.0003	0.0002
			$U = 500$ m/s				
0.5	1.9128	2104	0.5758	0.7486	0.5904	0.5295	0.4110
1.0	0.9564	2127	0.3092	0.3743	0.2952	0.2925	0.2268
2.0	0.4782	2132	0.1618	0.1871	0.1476	0.1552	0.1199
5.0	0.1913	2144	——	0.0749	0.0590	0.0647	0.0498
10	0.0956	2144	——	0.0374	0.0295	0.0328	0.0252
20	0.0478	2144	——	0.0187	0.0148	0.0165	0.0127
50	0.0191	2144	——	0.0075	0.0059	0.0066	0.0051
100	0.0096	2144	——	0.0037	0.0030	0.0033	0.0026
1000	0.0010	2144	——	0.0004	0.0003	0.0003	0.0003
			$U = 1000$ m/s				
0.5	3.8257	2502	0.5419	0.8886	0.6958	0.5400	0.5156
1.0	1.9128	2539	——	0.4443	0.3479	0.2951	0.2821
2.0	0.9564	2539	——	0.2222	0.1740	0.1558	0.1487
5.0	0.3826	2539	——	0.0889	0.0696	0.0647	0.0616
10	0.1913	2539	——	0.0444	0.0348	0.0328	0.0312
20	0.0956	2539	——	0.0222	0.0174	0.0165	0.0157
50	0.0383	2539	——	0.0089	0.0070	0.0066	0.0063
100	0.0191	2539	——	0.0044	0.0035	0.0033	0.0032
1000	0.0019	2539	——	0.0004	0.0003	0.0003	0.0003

[a]No vibrational excitation.

Table 4 Nusselt numbers for H_2O

			Nu				
Kn	*Re*	T_{ad}	DSMC	FM	FM*[a]	Kav	K–S
			$U = 100$ m/s				
0.5	0.3067	2002	0.4963	0.9702	0.6130	0.6208	0.5045
1.0	0.1534	2003	——	0.4851	0.3065	0.3586	0.2888
2.0	0.0767	2003	——	0.2426	0.1532	0.1951	0.1556
5.0	0.0307	2003	——	0.0970	0.0613	0.0826	0.0653
10	0.0153	2003	——	0.0485	0.0306	0.0421	0.0332
20	0.0077	2003	——	0.0243	0.0153	0.0213	0.0167
50	0.0031	2003	——	0.0097	0.0061	0.0086	0.0067
100	0.0015	2003	——	0.0049	0.0031	0.0043	0.0034
1000	0.0002	2003	——	0.0005	0.0003	0.0004	0.0003
			$U = 500$ m/s				
0.5	1.5337	2044	0.6842	1.0139	0.6382	0.6439	0.5500
1.0	0.7668	2067	0.3439	0.5070	0.3191	0.3643	0.3091
2.0	0.3834	2075	0.2112	0.2535	0.1595	0.1963	0.1653
5.0	0.1534	2064	——	0.1014	0.0638	0.0827	0.0691
10	0.0767	2064	——	0.0507	0.0319	0.0421	0.0351
20	0.0383	2064	——	0.0253	0.0160	0.0213	0.0177
50	0.0153	2064	——	0.0101	0.0064	0.0086	0.0071
100	0.0077	2064	——	0.0051	0.0032	00043	0.0036
1000	0.0008	2064	——	0.0005	0.0003	0.0004	0.0004
			$U = 1000$ m/s				
0.5	3.0674	2269	0.7200	1.1487	0.7157	0.6593	0.6548
1.0	1.5337	2242	——	0.5744	0.3578	0.3682	0.3640
2.0	0.7668	2242	——	0.2872	0.1789	0.1972	0.1937
5.0	0.3067	2242	——	0.1149	0.0716	0.0828	0.0808
10	0.1534	2242	——	0.0574	0.0358	0.0422	0.0410
20	0.0767	2242	——	0.0287	0.0179	0.0213	0.0207
50	0.0307	2242	——	0.0115	0.0072	0.0086	0.0083
100	0.0153	2242	——	0.0057	0.0036	0.0043	0.0042
1000	0.0015	2242	——	0.0006	0.0004	0.0004	0.0004

[a]No vibrational excitation.

Nu predictions from DSMC and the Kav and K–S correlations are presented in Figs. 5–7 for CO_2, H_2O, and N_2 as a function of *Re* at $Kn = \frac{1}{2}, 1, 2, 5$, and 10. CO results are not presented graphically, because they are essentially the same as the N_2 results. Calculations were done for U between 100 and 1000 m/s, resulting in a *Re* variation of an order of magnitude. DSMC data are shown by the symbols at *Re* corresponding to $U = 100$, 500, and 1000 m/s. The DSMC *Nu* values are sensitive to the value of T_{ad}. They are subject to large percentage errors at low U (or low *Re*). This accounts for most of the difference between DSMC and the correlations. The DSMC values of *Nu* are generally higher than the Kav and K–S correlations; however, inspection of Tables 1–4 shows that they are considerably smaller than the FM predictions of *Nu*. Both the Kav and K–S correlations give reasonable predictions of *Nu*. Note that *Nu* seems to vary almost linearly with *Kn*. Consequently, it may be possible to reduce the individual curves to a single line by multipling by Kn^{δ}, where δ is quite close to 1.

Figures 8–10 show comparisons of *Nu* from DSMC, FM, and FM* and the Kav and K–S correlations as a function of *Kn* for CO_2, H_2O, CO, and N_2 at $U = 500$ m/s. Note that Fig. 10 contains both the CO and N_2 data. The DSMC results and those of the Kav and K–S correlations are roughly the averages of the results for FM and FM*. The FM results become progressively worse as *Kn* decreases, as expected.

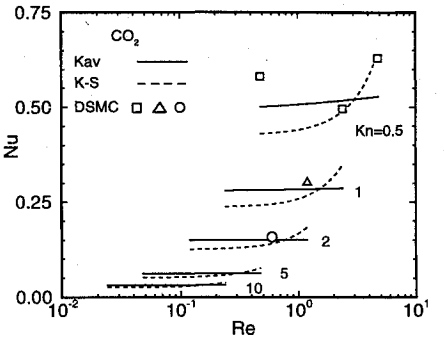

Fig. 5 Comparison of *Nu* from Kav and K–S correlations with DSMC predictions for CO_2 vs *Re*. $T_g = 2000$ K.

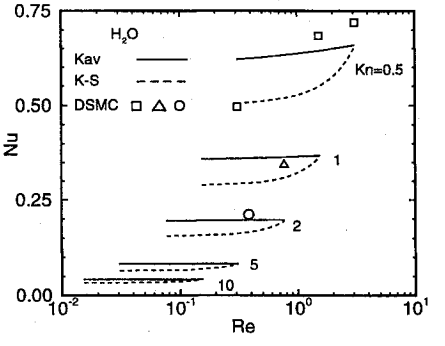

Fig. 6 Comparison of *Nu* from Kav and K–S correlations with DSMC predictions for H_2O vs *Re*. $T_g = 2000$ K.

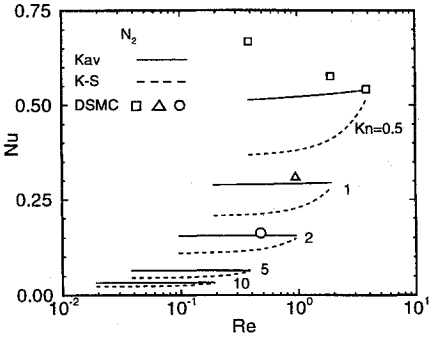

Fig. 7 Comparison of *Nu* from Kav and K–S correlations with DSMC predictions for N_2 vs *Re*. $T_g = 2000$ K.

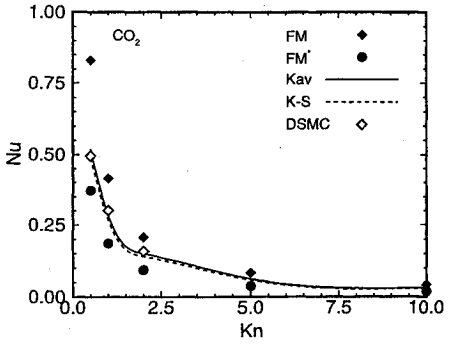

Fig. 8 Comparison of *Nu* from Kav and K–S correlations and FM, FM*, and DSMC predictions for CO_2 vs *Kn* at $U = 500$ m/s. $T_g = 2000$ K.

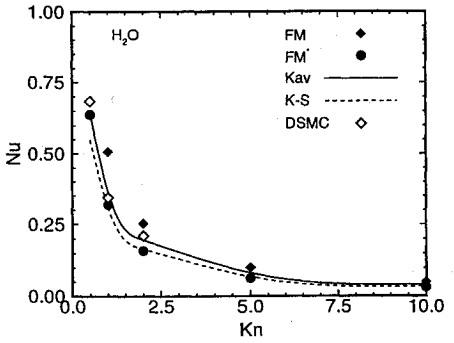

Fig. 9 Comparison of *Nu* from Kav and K–S correlations and FM, FM*, and DSMC predictions for H_2O vs *Kn* at $U = 500$ m/s. $T_g = 2000$ K.

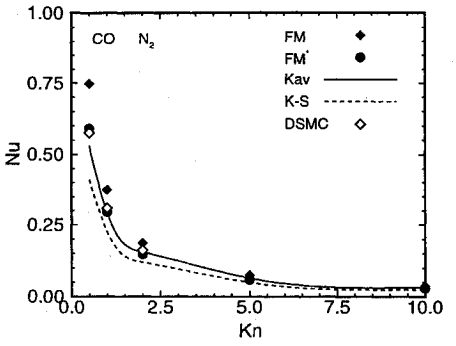

Fig. 10 Comparison of *Nu* from Kav and K–S correlations and FM, FM*, and DSMC predictions for CO and N_2 vs *Kn* at $U = 500$ m/s. $T_g = 2000$ K.

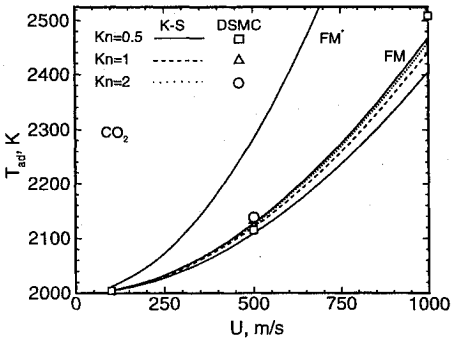

Fig. 11 T_{ad} for CO_2 vs U for $Kn = \frac{1}{2}$, 1, and 2 and for K–S correlation, DSMC, FM, and FM*. $T_g = 2000$ K.

Figures 11–14 show T_{ad} as a function of U for CO_2, H_2O, CO, and N_2, respectively. Data are shown for DSMC, the K–S correlation at $Kn = \frac{1}{2}$, 1, and 2, and FM and FM*. Vibrational excitation becomes more important as U increases. FM* predicts high values of T_{ad} because the gas energy cannot relax by exciting the vibrational energy modes. The DSMC calculations, FM predictions, and the K–S correlation agree well, even at low Kn.

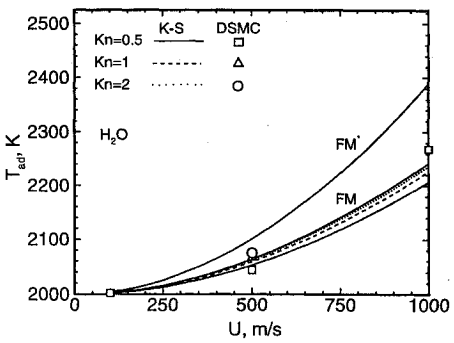

Fig. 12 T_{ad} for H_2O vs U for $Kn = \frac{1}{2}$, 1, and 2 and for K–S correlation, DSMC, FM, and FM*. $T_g = 2000$ K.

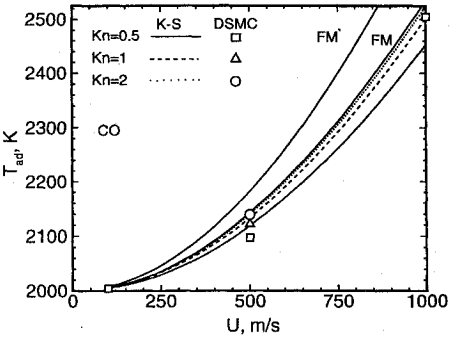

Fig. 13 T_{ad} for CO vs U for $Kn = \frac{1}{2}$, 1, and 2 and for K–S correlation, DSMC, FM, and FM*. $T_g = 2000$ K.

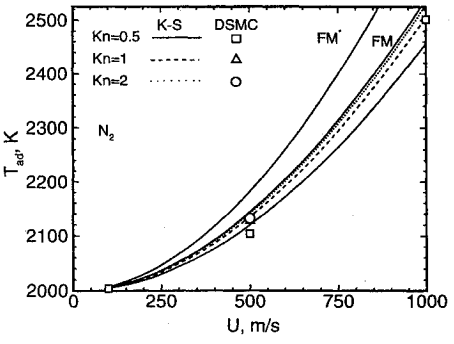

Fig. 14 T_{ad} for N_2 vs U for $Kn = \frac{1}{2}$, 1, and 2 and for K–S correlation, DSMC, FM, and FM*. $T_g = 2000$ K.

Conclusions

DSMC and FM methods have been used to predict the *Nu* of Al_2O_3 particles in a plume environment for a wide range of conditions. The gases considered were CO_2, CO, H_2O, and N_2. The gas temperature was 2000 K, and particle temperatures were 1500, 2000, and 2500 K. The relative velocities between the particles and the gas were 100, 500, and 1000 m/s, and Kn ranged from $\frac{1}{2}$ to 1000.

It is shown that the Kav and K–S correlations both yield good predictions of the high-temperature Nusselt number for each of the gases considered, even though both correlations were originally developed for air at temperatures near 300 K. Vibrational excitation of the gas molecules is shown to be important in determining accurate particle adiabatic wall temperatures at realistic plume thermodynamic conditions. The adiabatic wall temperature becomes more sensitive to the vibrational population as the relative velocity increases. To the authors' knowledge this research presents the first predictions of high-temperature Nusselt numbers and adiabatic wall temperatures for plume gases.

Acknowledgments

This research was performed under Subcontracts A93S-9 and A94S-24 with Sverdrup Technology, Inc., Arnold Air Force Base, Tennessee, and monitored by Robert A. Reed and Robert S. Hiers III. The authors wish to acknowledge the many helpful discussions

about DSMC with Richard G. Wilmoth of NASA Langley Research Center, Hampton, Virginia.

References

[1]Moylan, B., and Sulyma, P., "Investigation of Gas/Particle Heat Transfer Rates in Solid Rocket Motors," AIAA Paper 92-3619, July 1992.

[2]Kavanau, L. L., "Heat Transfer from Spheres to a Rarefied Gas in Subsonic Flow," *Transactions of the ASME*, Vol. 77, No. 8, 1955, pp. 617–623.

[3]Eckert, E. R. G., and Drake, R. W., *Heat and Mass Transfer*, 2nd ed., McGraw–Hill, New York, 1959, pp. 272–300.

[4]Sauer, F. M., "Convective Heat Transfer from Spheres in a Free Molecule Flow," *Journal of the Aeronautical Sciences*, Vol. 18, May 1951, pp. 353, 354.

[5]Oppenheim, A. K., "Generalized Theory of Convective Heat Transfer in a Free-Molecule Flow," *Journal of the Aeronautical Sciences*, Vol. 20, No. 1, 1953, pp. 49–58.

[6]Kays, W. M., and Crawford, M. E., *Convective Heat and Mass Transfer*, 2nd ed., McGraw–Hill, New York, 1980, pp. 304, 305.

[7]Koshmarov, Y. A., and Svirshevskii, S. B., "Heat Transfer from a Sphere in the Intermediate Dynamics Region of a Rarefied Gas," *Mekhanika Zhidkosti i Goza*, No. 2, March–April 1972, pp. 170–172; also *Fluid Dynamics*, Vol. 7, 1972, pp. 343–346.

[8]Hiers, R. S., III, private communication, Sverdrup Technology, Inc., Arnold AFB, TN, Sept. 1992.

[9]Bird, G. A., "Monte Carlo Simulation in an Engineering Context," *Rarefied Gas Dynamics*, edited by S. S. Fischer, Vol. 74, Progress in Astronautics and Aeronautics, AIAA, New York, 1981, pp. 239–255.

[10]Bird, G. A., *Molecular Gas Dynamics and the Direct Simulation of Gas Flows*, 1st ed., Oxford Univ. Press, New York, 1994.

[11]Fields, J. C., "Drag and Heat Transfer of Particles in Solid Rocket Plumes," M.S. Thesis, Dept. of Mechanical and Aerospace Engineering and Engineering Mechanics, Univ. of Missouri–Rolla, MO, Dec. 1994.

T. C. Lin
Associate Editor